

Enhancement of energy relaxation rates near metal-coated dielectric cylinders

G. D. Banyard, C. R. Bennett and M. Babiker

Department of Physics, University of York, Heslington, York YO10 5DD, England

Abstract

The electromagnetic modes and their field distributions are evaluated for a dielectric cylindrical structure embedded in another dielectric, with a thin metallic film at the cylinder/dielectric interface. These modes provide energy relaxation channels for excited dipole emitters located inside or outside the cylinder. Significantly, we find that the emission rate is sensitive to the magnitude of the electron density of the metallic film coating. For typical parameter values, we find large enhancements of the emission rate, which can be in excess of three orders of magnitude, relative to the case in the absence of the film, arising at specific ranges of electron density. The theory is shown to conform with known limits, including the high density (perfect conductor) limit and the large distance (unbounded bulk) limit. The implications of the predicted enhancement due to the metal coating for the purpose of guiding atoms within such microstructures are pointed out.

PACS Numbers: 34.50.Dy, 32.80.-t, 41.20.Jb, 42.50.-p

There is at present much interest in small (micrometre to nanometre) scale spherical [1,2] and cylindrical structures [3-12]. A problem of immediate interest in this context is the response of quantum systems to the electromagnetic fields supported by structures of this kind. We concentrate here on cylindrical structures, as these have featured more prominently in recent applications than spherical structures. Although some work on the coupling of fields to electric dipoles near dielectric cylinders has been reported recently using Green functions and other methods [8], the greater majority of reports have been concerned with cylindrical structures where the walls are totally impenetrable to electromagnetic fields of all frequencies. In particular, Ripplin and Knight [9] quantised the electromagnetic modes in hollow cylindrical waveguides with perfectly conducting walls and proceeded to calculate the decay rate of an oscillating electric dipole located inside the cylindrical guide. However, as we have just pointed out, dielectric cylindrical structures have also been the subject of investigation, especially in experimental contexts and there is now clear need for theoretical investigations appropriate for the more general situation, involving dielectric structures.

Furthermore, it has become clear that the presence of a thin metallic film as an overlayer on a planar dielectric structure can lead to a considerable enhancement of the electromagnetic fields [13-15]. For similar reasons it is envisaged that a metal-coated dielectric cylinder should exhibit enhanced electromagnetic fields. As far as the authors are aware, the effect of a thin metallic film coated at the cylinder surface on the electromagnetic properties of such a system have not been explored before, nor has the coupling of the electromagnetic modes, modified by the presence of the film, to quantum systems localised in the vicinity of the film. In particular, the characteristics of dipole emission and the parameters which control the enhancement need to be understood and quantified. The primary aim of this communication is to report the results of a study along these lines.

We consider a general system comprising a dielectric cylinder of radius R_0 and dielectric constant ϵ_1 embedded in a different material of dielectric constant ϵ_2 . A

thin film of a given metal is introduced at the cylindrical interface between the two dielectrics. The system is schematically shown in Fig.1(a) in which an emitter of electric dipole moment vector $\boldsymbol{\mu}$ and oscillation frequency ω_0 can be situated at arbitrary points inside the cylinder ($r_t \leq R_0$) or outside it ($r_t > a$) where R_0 is the cylinder radius and r_t is the cylindrical polar radial position of the dipole emitter.

The allowed electromagnetic field modes are evaluated using the photon tunneling technique [16]. Briefly, the photon tunneling procedure involves plane waves which can either be transverse magnetic (TM) or transverse electric (TE) incident within region 2 (outside the cylinder) at an azimuthal angle ϕ_0 . This is reflected and transmitted at the cylinder surface, producing appropriate linear combinations of TE and TM solutions at the different regions in a manner satisfying electromagnetic boundary conditions. For this, one needs to express the incoming plane wave form in terms of Bessel functions using the following identity in cylindrical coordinates $\mathbf{r} = (r_t, \phi, z)$ [16]

$$e^{i\mathbf{k}_2 \cdot \mathbf{r}} = \sum_{n=-\infty}^{\infty} J_n(k_{t2}r_t) e^{i[n(\phi-\phi_0-\pi/2)+k_z z]} \quad (1)$$

where k_2 is one of two wavevectors in the problem defined by

$$\mathbf{k}_i = (\mathbf{k}_{ti}, k_z); \quad k_i^2 = \frac{\omega^2 \epsilon_i}{c^2} \quad (i = 1, 2) \quad (2)$$

In addition to the continuity of the tangential components of the electric field vector at the cylinder interface, the second set of boundary conditions must ensure that all tangential magnetic field components experience a jump due to the conductivity σ associated with the metallic film coating

$$\sigma = \frac{in_s e^2}{m^*(\omega + i\gamma)} \quad (3)$$

Here n_s is the two-dimensional electron density of the film, e and m^* are the electron charge and effective mass, respectively, and $\gamma \ll \omega$ represents a small plasma loss term. This boundary condition can be expressed as [13]

$$\hat{\mathbf{r}}_t \times [\mathbf{H}(R_{0+}, \phi, z) - \mathbf{H}(R_{0-}, \phi, z)] = \sigma \mathbf{E}_{\parallel}(R_0, \phi, z) \quad (4)$$

where the magnetic field vectors are evaluated at $R_{0\pm}$ where the \pm subscripts imply that the radial coordinate approaches $r_t = R_0$ from outside the cylinder (+) and inside it (-). The resulting field distributions inside and outside the cylinder emerge in terms of a sum over Bessel functions, reflecting the cylindrical symmetry of the structure. There are four types of mode: propagating (k_{t1} and k_{t2} both real), evanescent (k_{t1} imaginary, k_{t2} real), guided (k_{t1} real, k_{t2} imaginary) and surface modes (k_{t1} and k_{t2} both imaginary), whose characteristics depend on the relative magnitudes of the dielectric functions ϵ_1 and ϵ_2 , as well as the electron density n_s of the metallic coating. Figure 1(b) schematically shows the spatial dependence of the four types of mode mentioned above in the region of the cylinder surface. Figure 2 displays the dispersion regions of the allowed modes in the ω versus k_z plot. The light lines corresponding to ϵ_1 and ϵ_2 are also shown. In general, the modes will have a mixture of both TE and TM characters. However, in the limit $n_s \rightarrow \infty$, corresponding to the perfect conductor case, they split into pure TE and pure TM forms [16].

The analytical expressions of the electric field distributions corresponding to the allowed modes are too complicated to be displayed in full in this communication. Here we give a brief description of the main features with reference to the z-component of the electric field vector of the evanescent mode. The spatial dependence of this field vector component, both inside and outside the cylinder, can be displayed in the form

$$\mathcal{E}_{e,z}(\mathbf{r}, \mathbf{k}_2, t) = \sum_{n=-\infty}^{\infty} \left[\alpha_n J_n(k_{t2}r_t)\theta(r_t - R_0) + \frac{\beta_n H_n(k_{t2}r_t)\theta(r_t - R_0)}{\Delta_n(k_2)} + \frac{\gamma_n I_n(\kappa_{t1}r_t)\theta(R_0 - r_t)}{\Delta_n(k_2)} \right] e^{i[n(\phi - \phi_0 - \pi/2) + k_z z - \omega t]} \quad (5)$$

where θ is the step function and J_n , H_n and K_n are Bessel functions, while $\kappa_{t1} = ik_{t1}$ with k_{t1} given by Eq.(2). The subscript e in the electric field z-component in Eq.(5) specifies the type of mode as the evanescent mode. The forms of the factors α_n , β_n , γ_n and Δ_n are determined by the field normalisation requirements and the boundary conditions, the latter giving β_n and γ_n in terms of α_n . Note that the relation $\Delta_n = 0$

constitutes the dispersion relation for the surface and guided modes when $\alpha_n = 0$ and γ_n is given in terms of β_n . Similar expressions exist for the other components of the field corresponding to this type and for the other types of mode. Formally, we write for the i th component of the quantised electric field vector

$$E_i(\mathbf{r}, t) = \sum_{\mathbf{k}_2, \eta} \{ \mathcal{E}_{\eta, i}(\mathbf{r}, \mathbf{k}_2, t) a(\mathbf{k}_2, \eta) + h.c. \} \quad (6)$$

where η specifies the type of mode ($\eta = e$ and $i \equiv z$ in Eq.(5)); $a(\mathbf{k}_2, \eta)$ is the annihilation operator for this type of mode. In the case of propagating and evanescent modes, the process of normalisation for the quantised fields is carried out for a plane wave in an infinite bulk of material 2 (i.e. as though the cylinder does not exist) to give α_n . For the surface and guided modes the quantisation process follows the familiar path to give β_n . It can be shown that the quantisation procedure amounts to determining normalisation factors from the condition

$$\epsilon_0 \int d^3 \mathbf{r} \mathcal{E}_\eta(\mathbf{r}, \mathbf{k}_2) \cdot \mathcal{E}_\eta^*(\mathbf{r}, \mathbf{k}_2) = \frac{1}{2} \hbar \omega(k_2, \eta) \quad (7)$$

where $\mathcal{E}_\eta(\mathbf{r}, \mathbf{k}_2)$ are the electric field vector functions associated with the quantised field mode of type η , frequency $\omega(k_2, \eta)$ and wavevector \mathbf{k}_2 .

The energy relaxation rate for the oscillating dipole is evaluated by application of the Fermi golden rule

$$\Gamma(\mathbf{r}) = \frac{2\pi}{\hbar^2} \sum_{\mathbf{k}_2, \eta} |\langle e; \{0\} | -\boldsymbol{\mu} \cdot \mathbf{E}(\mathbf{r}) | g; \{\mathbf{k}_2, \eta\} \rangle|^2 \delta(\omega_0 - \omega) \quad (8)$$

where $\mathbf{E}(\mathbf{r}, \mathbf{t})$ is the quantised electric field vector operator at the position of the electric dipole. The notation is such that $|e\rangle$ and $|g\rangle$ are the two quantum states representing the dipole system, $|\{0\}\rangle$ stands for the corresponding zero photon (vacuum) field state, $|\{\mathbf{k}_2, \eta\}\rangle$ is a single quantum field state of frequency $\omega(k_2, \eta)$ and η runs over the allowed types of mode.

The result emerging from Eq.(8) should be modified to take account of the local field correction [17] such that

$$\Gamma(\mathbf{r}) \rightarrow \Gamma(\mathbf{r}) \left\{ \frac{3\epsilon(\mathbf{r}, \omega)}{2\epsilon(\mathbf{r}, \omega) + 1} \right\}^2 \quad (9)$$

where

$$\epsilon(\mathbf{r}, \omega) = \epsilon_1 \theta(R_0 - r_t) + \epsilon_2 \theta(r_t - R_0) \quad (10)$$

The expressions arising from Eq.(8), together with Eq.(9), by necessity, require numerical evaluations, which permit the exploration of the changes in the characteristics of the system with varying cylinder radius, dipole frequency, dipole position inside and outside the cylinder and with varying metallic film electron density. The results are shown in Figs. 3 to 5.

Figure 3 exhibits the variations in the rate with the dipole radial position r_t for a cylinder of fixed radius $R_0 = 500\text{nm}$. The inset to the figure shows the variations corresponding to the limiting cases $n_s = 0$ (absence of the film) [8] and $n_s = \infty$ (perfectly conducting film) [9-11]. The values at $r_t = 0$ are for dipole position on the cylinder axis. On the opposite side, for r_t large ($r_t \gg R_0$), it is seen that all the curves converge to the same value corresponding to the rate of a dipole embedded in the infinite bulk of dielectric 2. In the vicinity of the film where $r_t \approx R_0$ marked variations can be seen, depending on the density of the film. For $n_s = 10^{20}\text{m}^{-2}$ there is considerable enhancement near the surface; at this density the dipole frequency is at resonance with that of a surface mode. This is followed by a marked reduction at $n_s = 10^{21}\text{m}^{-2}$. Further increase in the density to $n_s = 10^{22}\text{m}^{-2}$ results in the rate dipping dramatically to smaller values approaching zero at the surface, as one would expect in the perfect conductor (large density) limit, shown in the inset to Fig. 3. Note that, for this cylinder radius, in the large n_s limit the lowest order ($n = 0$) mode is the only mode allowed in a cylinder of impenetrable walls.

Figure 4 displays the variations of the emission rate with the film density n_s for a dipole oriented parallel to the axis. The oscillation frequency is such that $\hbar\omega_0 = 0.5\text{eV}$ and the radius of the cylinder is taken to be $R_0 = 500\text{nm}$. Note the sudden onset of the dip in the rate for the dipole at the centre of the cylinder and close to the surface at $r_t = 0.9R_0$. This sudden dip with increasing density is for all dipoles located inside

the cylinder and which oscillate at $\hbar\omega_0 = 0.5\text{eV}$. This feature can be explained by the fact that at such a low frequency the lowest order mode cannot be excited since the radius of the cylinder is below the cut-off condition $\lambda_0 > R_0$ that exists for a cylinder surrounded by a perfect conductor.

By contrast, Fig. 5 displays the variations corresponding to the case in Fig. 4, but for a dipole oscillating at frequency such that $\hbar\omega_0 = 1.5\text{eV}$. Note the appearance of the second peak at high density when the dipole is inside the cylinder near the surface (dashed curve) and also the finite values at high densities for a dipole inside the cylinder (dashed and solid curves). The finite values at high densities can be explained by the fact that the lowest order mode in the corresponding perfect conductor (cylindrical waveguide) case has a frequency below ω_0 and this provides the necessary decay channel leading to a finite emission rate. The second peak in the dashed curve (dipole near the surface) is due to the next order mode in a cylinder with impenetrable walls which, although it has a frequency just above ω_0 , is at resonance inside the cylinder with the incoming TM wave within a certain finite range of surface densities.

From these results one clearly concludes that the presence of the metallic film modifies the electromagnetic properties of the dielectric structure in a manner strongly dependent on the electron density of the metallic film. In particular, it can lead to a considerable enhancement of the spontaneous rate. The theory also reproduces various appropriate limits, most notably: the high n_s limit, corresponding to the perfect conductor case, the zero n_s limit, corresponding to the bare dielectric cylinder case and the limit when the dipole is far away from the cylinder, corresponding to an unbounded medium 2.

Cylindrical dielectric structures, are particularly interesting for use not just as electromagnetic waveguides [3-5], but also as atom guides, where the guiding mechanism is mainly controlled by excited cavity modes [6,7,9,10]. It is envisaged that the development of atom guides at such a small scale would lead to much desirable advancements

in atom lithography and should facilitate atomic physics research. As mentioned previously, the enhancement of the evanescent mode due to the introduction of the metallic film has been put to good use in the context of atom mirrors where an overlayer is deposited on the planar dielectric surface of the conventional layer structure. This has been shown, both experimentally and theoretically, to lead to a pronounced enhancement of the repulsive potential arising from the modified evanescent mode [12-14].

Similarly, the enhancement found here in the case of a metal-coated cylinder is envisaged to produce a repulsive force which acts on the atom near the film in a hollow cylindrical structure. This should lead to an efficient atom guide in such a manner which is dependent on the density of the metallic film. The role of the metallic film in aiding the guiding action in hollow metal-coated dielectric cylindrical guides is currently under investigation and the results will be reported in due course.

References

1. H. T. Dung, L. Knöll and D.-G. Welsch, *Phys. Rev. A* **64**, 013804 (2001)
2. M. A. Kaliteevski, S. Brand and R. A. Abram, *J. Mod. Optics.*, in press (2001)
3. Y. Jiang and J. Hacker, *Appl. Optics* **33**, 7431 (1994)
4. M. A. Kaliteevski, R. A. Abram, V. V. Nikolaev and J. S. Sokolovski, *J. Mod. Optics*, **43**, 875 (1999)
5. A. J. Ward and J. B. Pendry, *J. Mod. Opt.* **43**, 773 (1996)
6. J P Dowling and J Gea-Banacloche, *Adv. Atom Mol. Opt. Phys.* **37**, 1 (1997)
7. V. I. Balykin, *Adv. Atom. Molec. Opt. Phys.* **4**, 181 (1999)
8. N. Nha and W. Jhe, *Phys. Rev. A* **56**, 2213 (1997); W. Zakowicz and M. Janowicz, *Phys. Rev. A* **62**, 013820 (2000)
9. M. A. Rippin and P. L. Knight, *J. Mod. Opt.* **47**, 807 (1996)
10. S. Al-Awfi and M. Babiker, *Phys. Rev. A* **58**, 2274 (1998)
11. M. Babiker and S. Al-Awfi, *J. Mod. Optics* **48**, 847 (2001)
12. D. Müller, E. A. Cornell, D. Z. Anderson and E. R. I. Abraham, *Phys. Rev. A* **61**, 03341 (2000).
13. C R Bennett, J B Kirk and M Babiker, *Phys. Rev. A* **63**, 033405 (2001)
14. S Feron, J Reinhardt, S Leboutoux, O Gocreix, J Baudon, M Ducloy, J Robert, C Miniatura, S N Chormaic, H Haberland and V Lorent, *Opt. Commun.* **102**, 83 (1993)
15. T Esslinger, M Weidenmüller, A Hammerich and T W Hänych, *Opt. Lett.* **18**, 450 (1993)

16. A. Ishimaru, "Electromagnetic wave propagation, radiation and scattering" (Prentice Hall: New Jersey, USA 1991)
17. R. J. Glauber and M. Lewenstein, Phys. Rev. A **43**, 467 (1991)

Figure Captions

Figure 1

(a) A schematic drawing showing the dielectric cylinder of material 1 immersed in another dielectric material 2. A thin metallic film is coated at the cylinder surface. The dielectric constants are ϵ_1 and ϵ_2 and the dipole is denoted by an arrow. (b) Schematic representation of the spatial dependence of the four types of mode (propagating, evanescent, guided and surface modes) in the region of the cylinder surface.

Figure 2

The regions of dispersion of the allowed modes in the cylinder. The light lines for the bulk media 1 and 2 are shown for the $\epsilon_1 = 1$ and $\epsilon_2 = 4$ case. The left shaded region contains the propagating modes, the other shaded region contains the evanescent modes and the solid curves are the lowest orders of an infinite number of surface modes, the lowest in energy being the $n = 0$ mode and the arrow signifying increasing n .

Figure 3

Variations in the spontaneous emission rate with the dipole radial position r_t for a cylinder of fixed radius $R_0 = 500\text{nm}$. The oscillation frequency is taken to be such that $\hbar\omega_0 = 1.5\text{eV}$ and the dipole moment vector is oriented parallel to the cylinder axis. The other parameters are $\epsilon_1 = 1$ and $\epsilon_2 = 4$. The three curves correspond to different metallic film coating density: $n_s = 10^{20}\text{m}^{-2}$ (solid curve), $n_s = 10^{21}\text{m}^{-2}$ (dashed curve) and $n_s = 10^{22}\text{m}^{-2}$ (dot-dashed curve). The inset to the figure shows the variations corresponding to the limiting cases $n_s = 0$, absence of the film (solid curve), and $n_s = \infty$, perfectly conducting film (dashed curve).

Figure 4

Variations of the emission rate with the film density n_s for a dipole oriented parallel to the axis. The oscillation frequency is such that $\hbar\omega_0 = 0.5\text{eV}$ and the radius of the cylinder is taken to be $R_0 = 500\text{nm}$. The three curves are for three different positions of the dipole: $r_t = 0$, dipole at the centre (solid curve); $r_t = 0.9R_0$, dipole inside, near the film (dashed curve); and $r_t = 1.5R_0$, dipole outside the cylinder (dot-dashed curve).

Figure 5

Variations corresponding to the case in Fig. 4, but for a dipole oscillating at frequency $\hbar\omega_0 = 1.5\text{eV}$. The three curves correspond to three different positions of the dipole: $r_t = 0$, dipole at the centre (solid curve); $r_t = 0.9R_0$, dipole inside, near the film (dashed curve); and $r_t = 1.5R_0$, dipole outside the cylinder (dot-dashed curve).

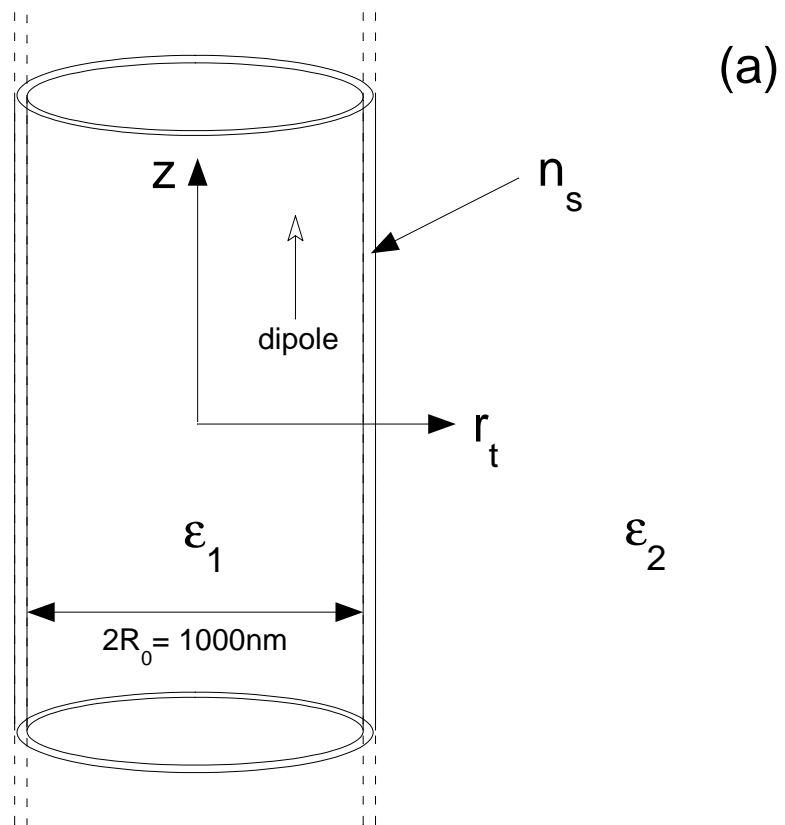
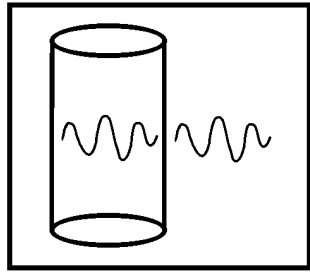
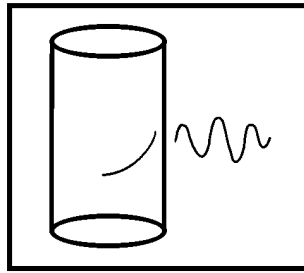


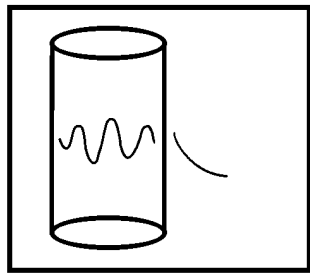
Figure 1a Banyard



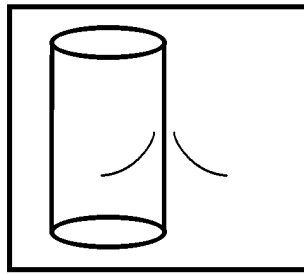
propagating



evanescent



guided



surface

(b)

Figure 1b Banyard

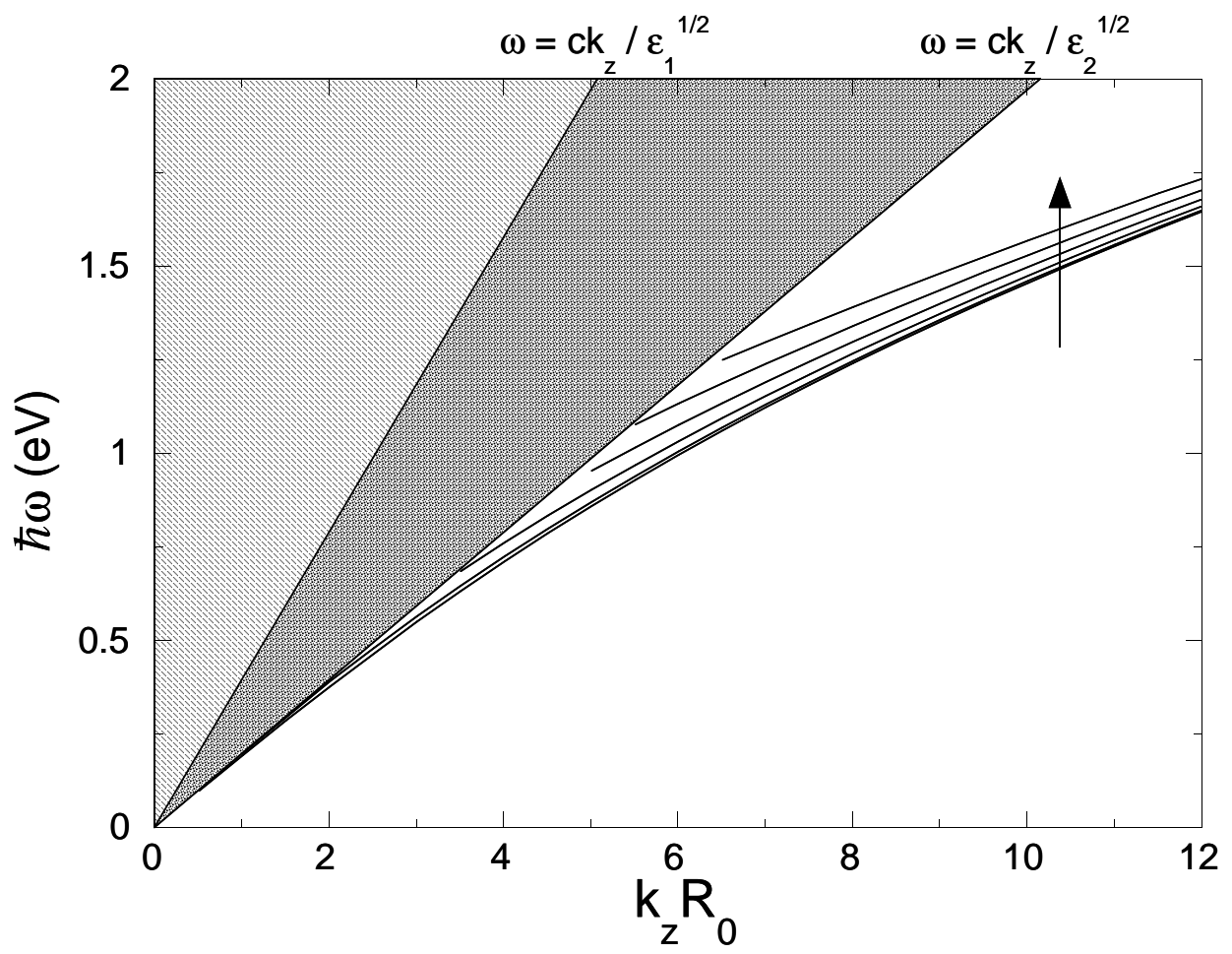


Figure 2 Banyard

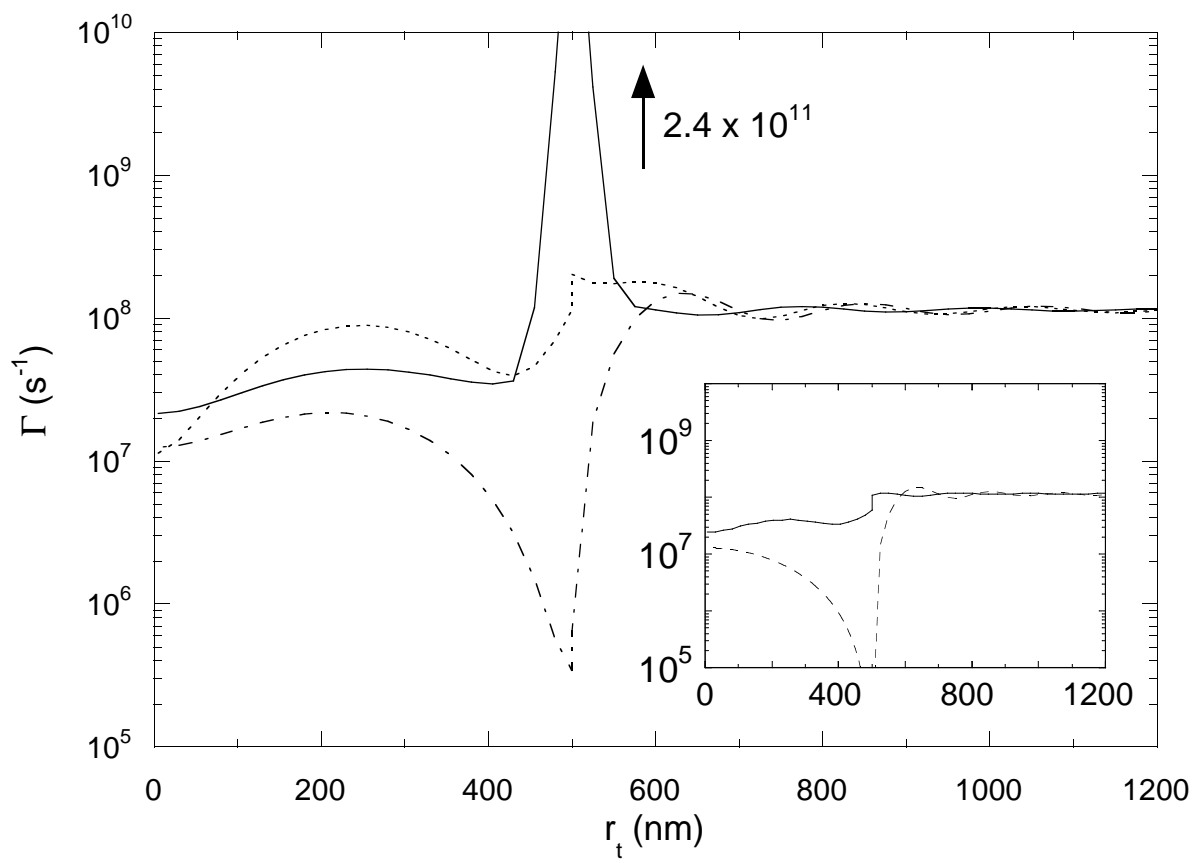


Figure 3 Banyard

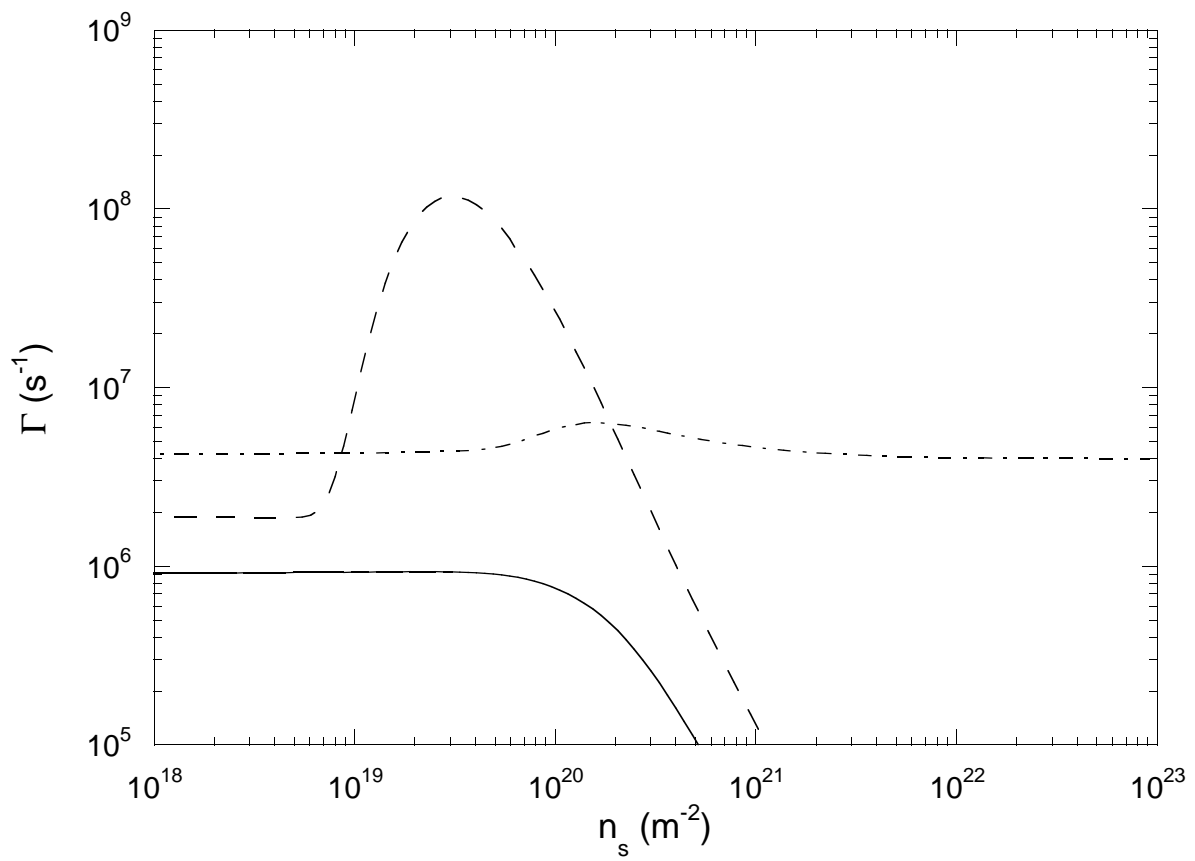


Figure 4 Banyard

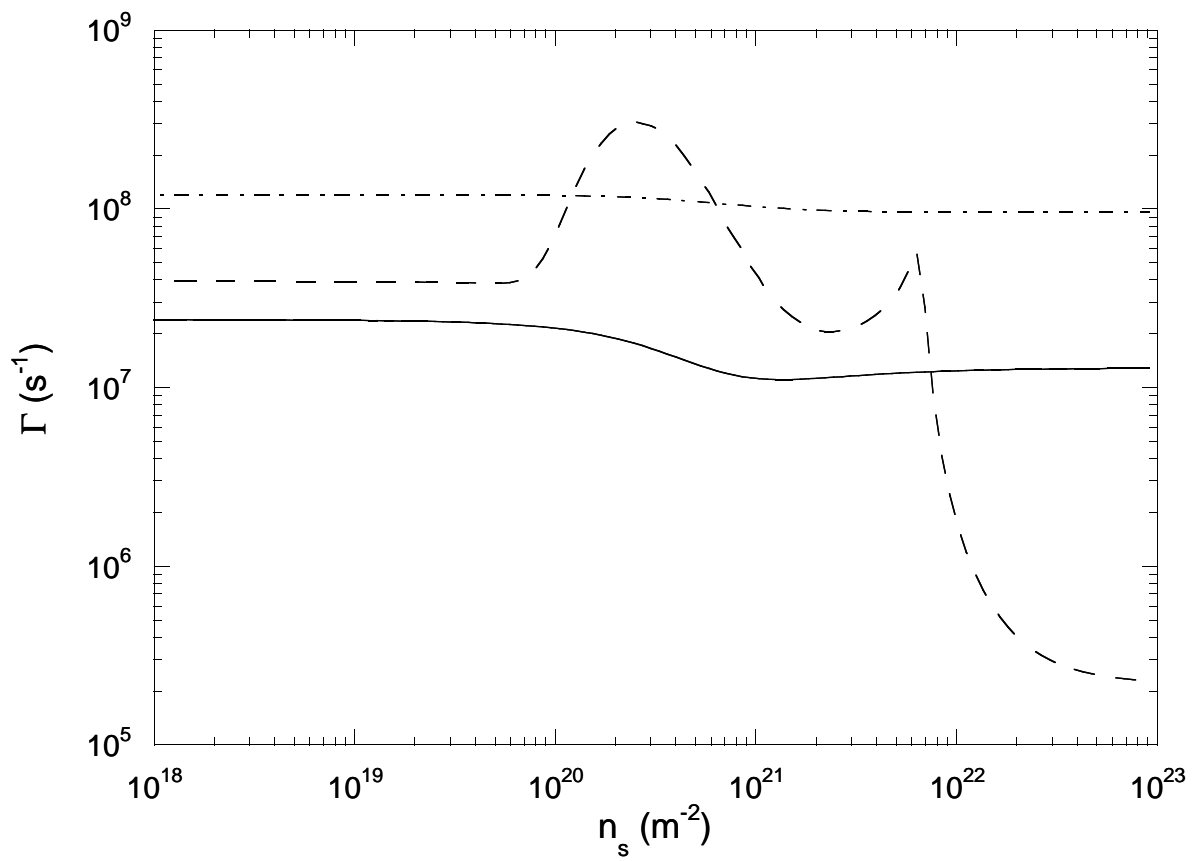


Figure 5 Banyard